DOI 10.1007/s10717-022-00428-x
Glass and Ceramics, Vol. 78, Nos. 11 – 12, March, 2022 (Russian Original, Nos. 11 – 12, November – December, 2021)

UDC 538.93

MICROSTRUCTURE FEATURES OF METAL-MATRIX COMPOSITES BASED ON THERMOELECTRIC BISMUTH TELLURIDE MATRIX AND FERROMAGNETIC FILLER

O. N. Ivanov,[1, 3] M. N. Yapryntsev,[2] A. E. Vasil'ev,[1] M. V. Zhezhu,[2] V. Yu. Novikov,[1] and E. P. Dan'shina[1]

Translated from *Steklo i Keramika*, No. 11, pp. 23 – 29, November, 2021.

The formative predictables of the microstructure of metal-matrix composites, obtained using spark plasma sintering and consisting of polycrystalline thermoelectric bismuth telluride Bi_2Te_3 (composite matrix) and a ferromagnetic filler (Ni or Fe), were examined. It was determined that, in the course of spark plasma sintering, filler inclusions in the form of locally gradient inclusions of the nucleus–shell type (Ni@$NiTe_2$ and Fe@$FeTe_2$) are formed and randomly distributed in the Bi_2Te_3 textured matrix. The basic parameters of the microstructure of composites (inclusion size and extent of texturing of the matrix) strongly depend on the filler content.

Key words: metal-matrix composites, spark plasma sintering, thermoelectric properties, texturing, locally gradient inclusions.

Composite materials, or composites, consist of two or more components differing in their physical and/or chemical properties [1, 2]. A composite consists of a matrix and a filler, which are its essential structural elements. As a rule, the filler is added to improve certain properties of the matrix material. Ordinarily, any properties of a composite which are of practical importance surpass the corresponding properties of its individual components. In addition, even new properties which are uncharacteristic for the components themselves can appear in the composite.

The specific properties of composites of different classes are mainly determined by the properties of the matrix material and the filler material as well as by the size, shape, dimensionality, concentration, and distribution of filler inclusions. A class of composites that is important from the applied standpoint is metal-matrix composites consisting of a ceramic matrix (Al_2O_3, ZrO_2, SiC, etc.) and a metal filler (Cr, Ti, Al, etc.) [3 – 5]. The introduction of a metal filler increases strength, wear-resistance, and heat resistance and improves the anticorrosive properties of metal-matrix composite composites. For this reason such metal-ceramic composites are customarily structural materials widely used in aircraft construction, automotive and mechanical engineering, and so on [1].

In a number of cases metal-matrix composites are developed in order to improve their functional (mainly electrical or magnetic) properties [6]. In particular, nowadays, as a promising scientific approach to thermoelectric materials science, a method of obtaining composites based on a conventional thermoelectric material, playing the role of a ceramic (polycrystalline) matrix, and a ferromagnetic metal filler (transition *d*-metals) is being used [7 – 11].

In such composites the introduction of a ferromagnetic metal filler can improve the thermoelectric properties — electrical conductivity, thermoEMF, and thermal conductivity — and, consequently, raise the thermoelectric figure of merit of the matrix material via the implementation of specific physical mechanisms determined by both the properties, size, and structure of the inclusions of the filler itself as well as the properties matrix/filler interfaces. As with customary composites, the thermoelectric properties of composites with a metal ferromagnetic filler will be largely determined by features of their microstructure: grain size, type and degree of grain ordering, size, shape, and internal structure of filler inclusions, and inclusion distribution in the matrix (ordered or random).

[1] V. G. Shukhov Belgorod State Technological University, Belgorod, Russia.
[2] Belgorod State National Research University, Belgorod, Russia.
[3] E-mail: Ivanov.Oleg@bsu.edu.ru.

The purpose of the present work was to establish the formative predictables of the microstructure of metal-matrix composites obtained using spark plasma sintering and consisting of polycrystalline thermoelectric bismuth telluride Bi_2Te_3 (matrix of the composite) and a ferromagnetic filler (Ni, Curie temperature $T_C = 627$ K, or Fe, $T_C = 1043$ K). Bi_2Te_3 itself is one of the boundary components in solid solutions $Bi_2Te_{3-x}Se_x$ and $Bi_{2-x}Sb_xTe_3$, which are used to produce different low-temperature thermoelectric generation and refrigeration devices [12]. However, the thermoelectric figure of merit ZT of bismuth telluride is not very high ($ZT \le 1$). The point of developing composites based on a Bi_2Te_3 matrix with a ferromagnetic filler is to improve the thermoelectric properties of the matrix material.

SAMPLE PREPARATION AND INVESTIGATIVE PROCEDURES

In the course of this work, samples of metal-matrix composite composites were obtained in the systems $Bi_2Te_3 + x$Ni and $Bi_2Te_3 + x$Fe with different atomic content of the filler ($x = 0$, 0.5, 0.75, 1.0, 1.25, and 1.5%). Composites were obtained by subjecting mixtures of initial powders of Bi_2Te_3 and Ni or Bi_2Te_3 and Fe taken in the required ratio to spark plasma sintering (SPS-25/10 system) at 40 MPa and temperature 573 K for 2 min. The initial Bi_2Te_3 powder was obtained by dissolving the precursors (high purity) Bi_2O_3, SeO_2, and TeO_2, taken in a stoichiometric ratio, in ethylene glycol with the addition of a small amount of an alkaline agent (KOH) for pH control. The resulting solution was poured into a flask and heated to boiling. After the water evaporated, the flask with the solution was hermetically sealed with a reflux condenser and kept at temperature 458 K for 4 h, and then the resulting suspension was cooled to room temperature. Further, the powder was purified by filtration and triple washing with ethanol and acetone and dried in an argon atmosphere at 523 K for 2 h.

To synthesize Ni powder, first, 5 g of $Ni(NO_3) \cdot 6H_2O$ were dissolved in 400 ml of ethylene glycol. Then 10 g of KOH was added to the solution. The mixture was heated to 353 K, stirring intensively until a homogeneous state was reached. The resulting sol was cooled to room temperature and then hydrazine hydrate was added slowly. The reaction mixture was heated to 373 K and kept for 1 h until completion of the reduction process $Ni^{2+} \rightarrow Ni^0$. The resulting Ni powder was collected with a neodymium magnet and washed with ethanol and acetone to remove organic impurities. In contrast to independently synthesized Bi_2Te_3 and Ni powders, a commercial powder with purity 99.995% was used as the initial Fe powder (Khimkraft LLC, Kaliningrad, Russia). Prior to spark plasma sintering, the initial powders of Bi_2Te_3 and Ni or Bi_2Te_3 and Fe, taken in a ratio corresponding to a certain value of x, were thoroughly mixed in a planetary mill for 30 min.

X-ray phase analysis of the initial powders and bulk samples of the composites was performed with a Rigaku SmartLab x-ray diffractometer (CuK_α radiation). The morphology of the initial Bi_2Te_3 and Ni powders was studied by means of transmission electron microscopy (TEM) using a Jeol 2100 microscope. The morphological features of the initial Fe powder and the grain structure of the bulk samples of the composites were studied by means of scanning electron microscopy (SEM) with a Quanta 600 microscope. The same microscope was used to study the elemental composition (EDS — energy-dispersive x-ray spectroscopy), and the phase contrast (BSE — back-scattered electrons) of the surface of the samples was determined.

EXPERIMENTAL RESULTS

The synthesized Bi_2Te_3 powder corresponded to a hexagonal phase ($R3m$ space symmetry group and crystal lattice parameters $a = 0.4354$ nm and $c = 3.035$ nm) and consisted mainly of hexagonal plates of average size several hundred nanometers and thickness about 100 nm. The synthesized Ni powder was a face-centered cubic phase $Fm3m$ with lattice parameter $a = 0.3525$ nm and consisted of almost spherical agglomerated formations with diameter 150 – 200 nm. Individual particles, several tens of nanometers in size, forming agglomerates had an irregular shape. Agglomeration of Ni particles can be associated with their ferromagnetic interaction. The commercial Fe powder likewise was uniphase (space symmetry group $Im3m$ ($a = 0.2867$ nm) and consisted of individual spherical particles with average diameter about 3 μm.

The data presented in Fig. 1 confirm the formation of the required matrix-filler microstructure in the composites being developed.

Spark plasma sintering of the initial Bi_2Te_3 and Ni or Bi_2Te_3 and Fe powders (SEM images of individual powder particles are shown on the left-hand side of the figure) indeed leads to the formation of a microstructure represented by filler inclusions embedded in the matrix of the composites (BSE images of polished surfaces of Bi_2Te_3 + 0.5 at.% Ni and Bi_2Te_3 + 0.5 at.% Fe are displayed in the right-hand part of the figure). In the BSE images, filler inclusions are shown as small, dark-gray islands randomly distributed in a light-gray matrix. Mapping of the distribution of different elements over the surface of the developed metal-matrix composite composites, performed by means of EDS, made it possible to determine their elemental composition.

The results of mapping Te, Bi, and Fe distributed over the surface of the Bi_2Te_3 + 0.5 at.% Fe are displayed in Fig. 2.

It is clear that Te and Bi are uniformly distributed within the light-gray matrix, while Fe is present only in dark-gray filler inclusions. As will be shown below, the composition and structure of these inclusions are rather complex. Assuming that there is no chemical interaction between the ma-

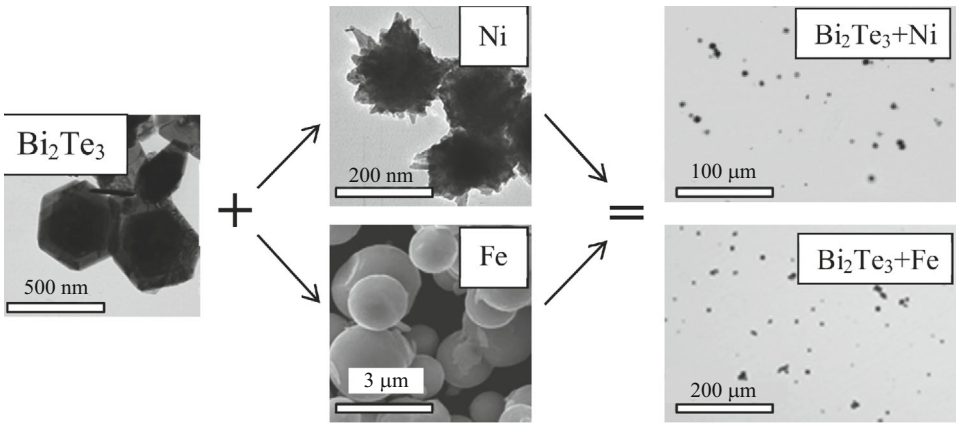

Fig. 1. Formation of the matrix-filler structure of the composites Bi_2Te_3 + 0.5 at.% Ni and Bi_2Te_3 + 0.5 at.% Fe (BSE images on the right-hand size) in the course of spark plasma sintering of the initial Bi_2Te_3, Ni, and Fe powders (SEM images on the left-hand side).

trix and filler materials, the phase composition of the developed metal-matrix composite composites should be a simple superposition of the matrix and filler phases. Then the diffractogram of the composite should also be a superposition of the diffractograms of the matrix and filler materials. It should be noted that the diffraction peaks of the Ni and Fe phases in the diffraction patterns of the composites are weak (because of the low content of these phases); moreover, most of these peaks are completely or partially obscured by the diffraction peaks of the Bi_2Te_3 phase, which makes reliable identification of the phase composition of the composites difficult.

However, at least for Bi_2Te_3 + xNi the phase composition of composites can be determined reliably enough. For these composites some diffraction peaks of the Ni phase can be resolved. Likewise, it was also determined that, in addition to the peaks of the Bi_2Te_3 and Ni phases, the diffraction patterns of these composites include additional peaks corresponding to a new phase formed during spark plasma sintering of a mixture of the initial Bi_2Te_3 and Ni powders. The indicated change in the phase composition for the composite with x = 1.25 at.% is illustrated in Fig. 3.

It is clear that the diffractogram of the composite comports with three phases: a dominant matrix phase Bi_2Te_3 and a weakly expressed phase of the Ni filler (triangles mark the diffraction peaks of this phase), which correspond to the initial powders, as well as the new phase (circles mark the peaks of this phase).

The new phase corresponds to the compound $NiTe_2$, having the trigonal spatial symmetry group $P\bar{3}m1$ and lattice parameters a = 0.3895 nm and c = 0.5470 nm.

The inclusions in the composites being developed possess a nucleus–shell structure. This structure is most clearly observed for inclusions of the Bi_2Te_3 + xNi composite (in these inclusions the nucleus and shell fractions are approximately comparable), while for of the Bi_2Te_3 + xFe inclusions the nucleus–shell structure is much less pronounced (the overwhelming share of the inclusion falls on the nucleus). Typical BSE images of nucleus–shell inclusions in the composites Bi_2Te_3 + xNi and Bi_2Te_3 + xFe are shown in Fig. 4.

To identify the elemental composition of these inclusions by means of EDS method, the distribution of the corresponding chemical elements along the lines intersecting the inclusions was studied. On the basis of an analysis of the scanning profiles of various elements it was found that the nucleus of an inclusion consists of Ni (in the Bi_2Te_3 + xNi composite) or Fe (in the Bi_2Te_3 + xFe composite). The shell of the inclusions contains Ni and Te atoms (in the Bi_2Te_3 + xNi composite) or Fe and Te (in the Bi_2Te_3 + xFe composite).

Far from inclusions all filler atoms are absent in composites of both types, and Bi and Te are uniformly distributed. Since a gradient distribution of elements exists in inclusions it is logical to call such inclusions locally gradient inclusions.

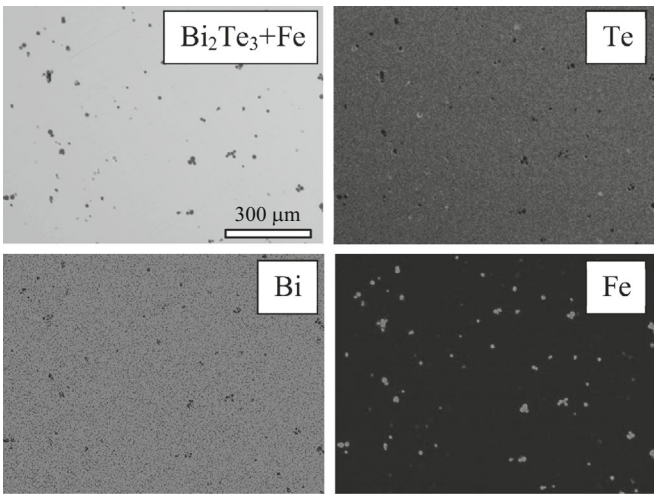

Fig. 2. BSE image of the polished surface of the metal-matrix composite composite Bi_2Te_3 + 0.5 at.% (atomic) Fe and the corresponding EDS maps of Te, Bi, and Fe distributions over the surface.

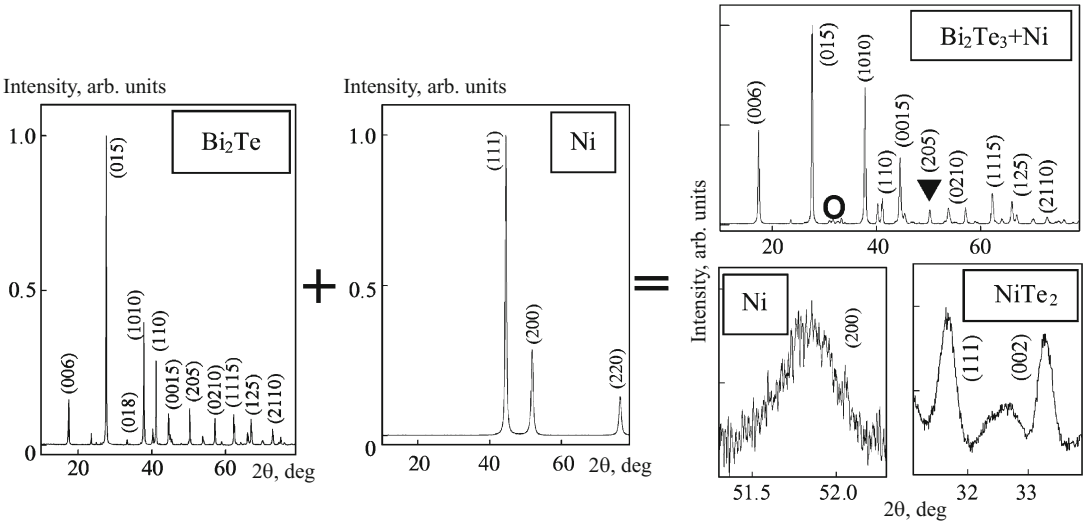

Fig. 3. Change in the phase composition of the composite Bi_2Te_3 + 1.5% (atomic) Ni during spark plasma sintering of the initial Bi_2Te_3 and Ni powders.

Since a new phase $NiTe_2$ is formed in the $Bi_2Te_3 + x$Ni composite during spark plasma sintering (see Fig. 3), and taking into account the identification of the elemental composition of inclusions in this composite (see Fig. 4), it can be concluded that In this case the shell of the composite corresponds precisely to the $NiTe_2$ compound (Ni@$NiTe_2$ inclusions). Although a new phase similar to $NiTe_2$ is not observed in the diffractogram of the $Bi_2Te_3 + x$Fe composite the inclusions for this composite also have a nucleus–shell structure with gradient variation of the elemental composition, similar to Ni@$NiTe_2$ inclusions in the $Bi_2Te_3 + x$Ni composite. Then it can be assumed that the shell in the inclusions of the $Bi_2Te_3 + x$Fe composite corresponds to the $FeTe_2$ phase, i.e. these inclusions can be thought of as Fe@$FeTe_2$ inclusions.

The formation of $NiTe_2$ or $FeTe_2$ shells surrounding Ni or Fe nuclei, respectively, is associated with high-temperature diffusion redistribution of matrix atoms and initial filler inclusions in the course of spark plasma sintering of initial powders. This redistribution is accompanied by a chemical reaction leading to the formation of the new compounds $NiTe_2$ or $FeTe_2$. It is obvious that the $NiTe_2$ compound is formed more quickly, since the shell in the Ni@$NiTe_2$ inclusions is larger than in the Fe@$FeTe_2$ inclusions. The difference in the sizes of the shells of inclusions in the composites $Bi_2Te_3 + x$Ni and $Bi_2Te_3 + x$Fe could be associated with different values of the diffusion coefficient of Ni and Fe and the activation energy of the chemical reactions Ni → $NiTe_2$ and Fe → $FeTe_2$. Filler inclusions for both types of composites are several microns in size, have nearly spherical shapes, and can be visualized not only on BSE images (see Fig. 4) but also on the corresponding SEM images (Fig. 5).

Spark plasma sintering of samples of the composites made from the initial powders leads to the development of strong texturing in the samples, which is easily observed on SEM images of the grain structure obtained from a cleaved surface oriented perpendicularly and parallel to the direction of pressure application during spark plasma sintering.

The texturing of the samples is associated with the preferential ordering of grains in a plane oriented perpendicular to the direction of pressure application during sintering (this direction is the texture axis). Texture formation is a typical phenomenon observed in Bi_2Te_3-based polycrystalline com-

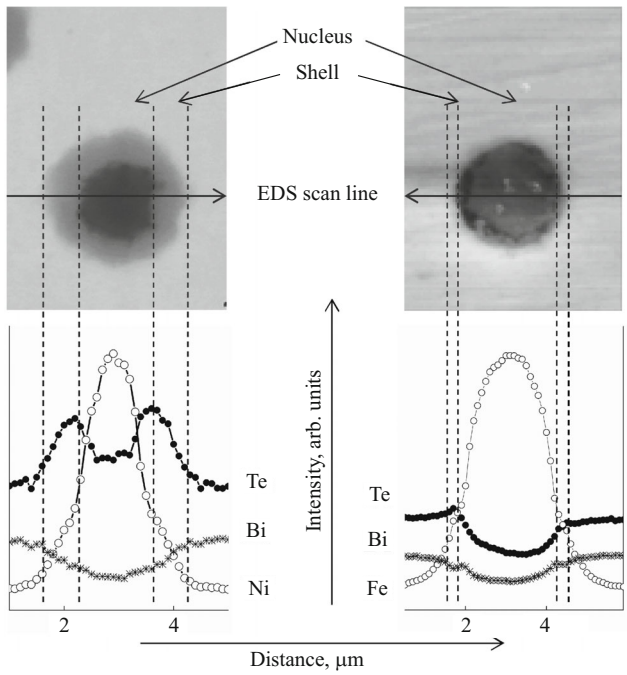

Fig. 4. BSE images of filler inclusions and scanning profiles of various elements taken along the line intersecting the inclusions for the Bi_2Te_3 + Ni (left-hand side) and Bi_2Te_3 + Fe (right-hand side) composites.

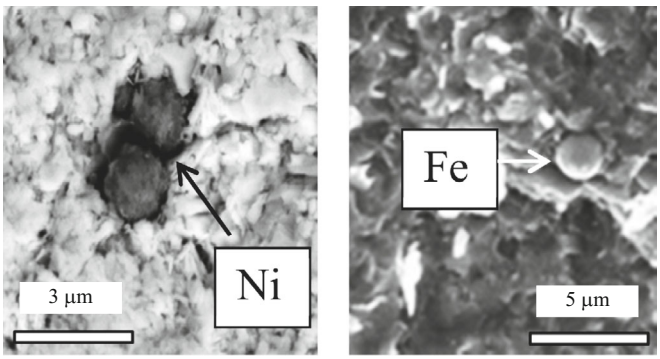

Fig. 5. SEM images of Ni inclusions in the Bi_2Te_3 + 0.5 at.% Ni (left-hand side) and Fe inclusions in the Bi_2Te_3 + 0.5 at.% Fe composite (right-hand side).

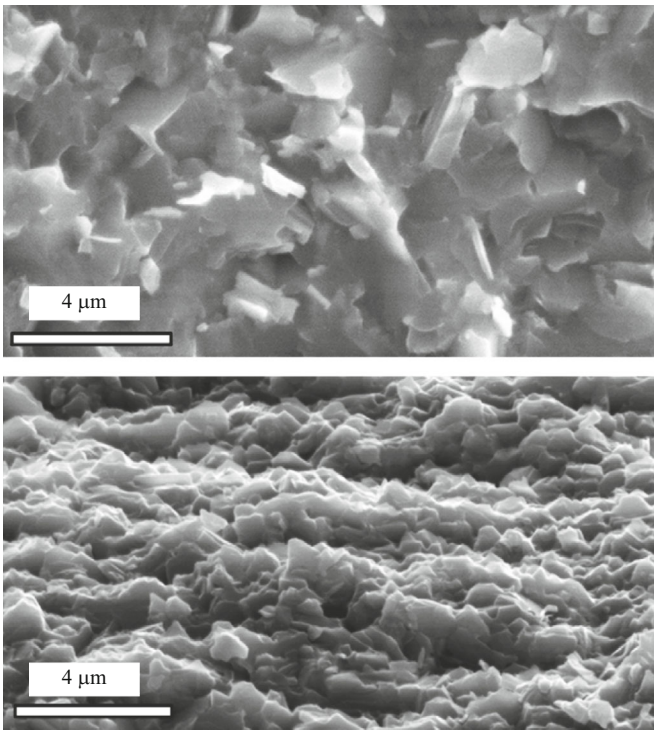

Fig. 6. SEM images of the grain structure of the composite Bi_2Te_3 + 0.5 at.% Fe obtained from surfaces oriented perpendicular (top) and parallel (bottom) to the direction of pressure application during spark plasma sintering.

pounds obtained using various technological methods based on uniaxial pressing of initial powders [13 – 17]. SEM images of perpendicular and parallel surfaces for the composite Bi_2Te_3 + 0.5 at.% Fe are shown in Fig. 6.

The grain structure is a lamellar structure with the lamellar layers lying in a plane perpendicular to the direction of pressure application. The lamellar layers consist of grains elongated in a plane parallel to the direction of pressure application (SEM image of a parallel surface).

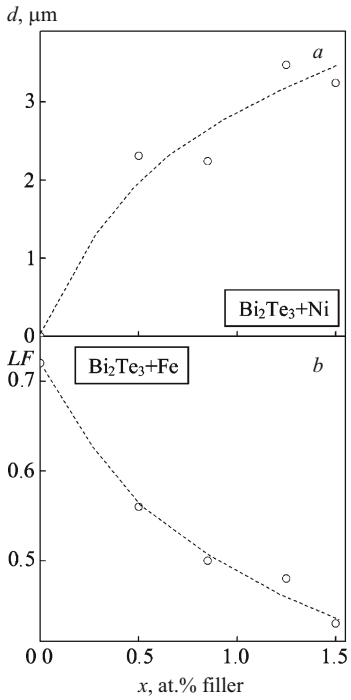

Fig. 7. Influence of the filler content on the size of Ni@$NiTe_2$ inclusions in the Bi_2Te_3 + Ni composite (*a*) and the Lotgering factor for the Bi_2Te_3 + Fe composite (*b*).

The grain structure in the SEM image of the perpendicular surface is represented by randomly oriented grains of irregular shape and size ≤ 1 μm.

It was determined that both the degree of texturing and the size of the inclusions in composites depend on the filler content. The results of a detailed study of the effect of the filler content on the microstructure and thermoelectric properties of composites will be reported in a separate article. Here, as preliminary results demonstrating the existence of such an effect, we offer the dependence of the size *d* of Ni@$NiTe_2$ inclusions on the Ni content in the Bi_2Te_3 + *x*Ni composite (Fig. 7*a*) and the dependence of the degree of texturing, determined using the Lotgering factor *LF* [17], on the Fe content in the Bi_2Te_3 + *x*Fe composite (Fig. 7*b*). Generally, *d* trends upward with increasing Ni content and the Lotgering factor gradually increases with increasing Fe content.

CONCLUSIONS

Spark plasma sintering of powder mixtures of thermoelectric Bi_2Te_3 and ferromagnetic metal Ni or Fe was used to obtain metal-matrix composite composites Bi_2Te_3 + *x*Ni and Bi_2Te_3 + *x*Fe was used to obtain. Filler inclusions in the form of locally gradient nucleus–shell inclusions (Ni@$NiTe_2$ and Fe@$FeTe_2$) randomly distributed in the textured Bi_2Te_3 matrix are produced. The nucleus–shell inclusions are formed as a result of high-temperature diffusion redistribution of matrix

and filler atoms during sintering, which is accompanied by the initiation of the chemical reactions $Ni \rightarrow NiTe_2$ and $Fe \rightarrow FeTe_2$. The microstructure parameters of the composites, such as the extent of texturing of the matrix and the size of the inclusions, strongly depend on the filler content.

This work was performed with the financial support of the RF Ministry of Education and Science under project No. 0625-2020-0015.

REFERENCES

1. Yu. A. Kurganov and A. G. Kolmakov, *Metal-Matrix Composite Materials for Construction* [in Russian], Izd. MGTU im. N. É. Baumana, Moscow (2015).
2. O. V. Mukbaniani, D. Balkose, H. Susanto, and A. K. Haghi (eds.), *Composite Materials for Industry, Electronics, and the Environment: Research and Applications*, Apple Academic Press, Palm Bay (2020).
3. A. X. Chen, C. Yang, R. H. Wang, et al., "Effect of raw materials on the properties of coated Al_2O_3–Al metal-matrix composite materials via vacuum sintering method," *Key Eng. Mater.*, **858**, 53 – 58 (2020).
4. J. F. Xu, G. Y. Liu, L. Tang, et al., "Synthesis and electrical properties of Mo–ZrO_2 metal-matrix composite," *Adv. Mater. Res.*, **311** – **313**, 2121 – 2126 (2011).
5. S. Ordońez, L. Carvajal, V. Martínez, et al., "Fracture toughness of SiC–Cu based alloys metal-matrix composites," *Mater. Sci. Forum*, **498 – 499**, 350 – 356 (2005).
6. A. Ali and A. Andriyana, "Properties of multifunctional composite materials based on nanomaterials: a review," *RSC Adv.*, **10**, 16390 – 16403 (2020).
7. W. Zhao, Z. Liu, P. Wei, et al., "Magnetoelectric interaction and transport behaviors in magnetic nanocomposite thermoelectric materials," *Nat. Nanotechnol*., **12**, 55 – 60 (2017).
8. W. Zhao, Z. Liu, Z. Sun, et al., "Superparamagnetic enhancement of thermoelectric performance," *Nature*, **13**, 247 – 251 (2017).
9. R. Lu, J. S. Lopez, Y. Liu, et al., "Coherent magnetic nanoinclusions induce charge localization in half-Heusler alloys leading to high Tc ferromagnetism and enhanced thermoelectric performance," *J. Mater. Chem. A*, **7**, 1095 – 11103 (2019).
10. M. Yaprintsev, A. Vasil'ev, O. Ivanov, et al., "Enhanced thermoelectric efficiency of the bulk composites consisting of 'Bi_2Te_3 matrix' and 'Ni@$NiTe_2$ filler inclusions'," *Scr. Mater.*, **194**, 113710-1-4 (2021).
11. M. Yaprintsev, A. Vasil'ev, O. Ivanov, et al., "Forming the locally gradient Ni@$NiTe_2$ domains from initial Ni inclusions embedded into thermoelectric Bi_2Te_3 matrix," *Mater. Lett*., **290**, 129451-1-4 (2021).
12. H. J. Goldsmid, "Bismuth telluride and its alloys as materials for thermoelectric generation," *Mater.*, **7**, 2577 – 2592 (2014).
13. S. D. Bhame, D. Pravarthana, W. Prellier, and J. G. Noudem, "Enhanced thermoelectric performance in spark plasma textured bulk *n*-type $Bi_2Te_{2.7}Se_{0.3}$ and *p*-type $Bi_{0.5}Sb_{1.5}Te_3$," *Appl. Phys. Lett*., **102**, 2190-1-3 (2013).
14. X. A. Fan, J. Y. Yang, R. G. Chen, et al., "Characterization and thermoelectric properties of *p*-type 25% Bi_2Te_3 – 75% Sb_2Te_3 prepared via mechanical alloying and plasma activated sintering," *J. Phys. D. Appl. Phys*., **39**, 740 – 745 (2006).
15. A. Vasil'ev, M. Yaprintsev, O. Ivanov, and E. Danshina, "Anisotropic thermoelectric properties of $Bi_{1.9}Lu_{0.1}Te_{2.7}Se_{0.3}$ textured via spark plasma sintering," *Sol. St. Sci*., **84**, 28 – 43 (2018).
16. M. Yaprintsev, A. Vasil'ev, and O. Ivanov, "Thermoelectric properties of the textured $Bi_{1.9}Gd_{0.1}Te_3$ compounds spark-plasma-sintered at various temperatures," *J. Europ. Cer. Soc.*, **40**, 742 – 750 (2020).
17. O. Ivanov, M. Yaprintsev, and A. Vasil'ev, "Comparative analysis of the thermoelectric properties of the non-textured and textured $Bi_{1.9}Gd_{0.1}Te_3$ compounds," *J. Sol. St. Chem*., **290**, 121559-1-10 (2020).